3D macroporous boron-doped diamond electrode with interconnected liquid flow channels: A high-efficiency electrochemical degradation of RB-19 dye wastewater under low current

Ruiqiong Mei[a,1], Qiuping Wei[a,1,*], Chengwu Zhu[a], Wentao Ye[a], Bo Zhou[b], Li Ma[a,*], Zhiming Yu[a], Kechao Zhou[a,*]

[a] State Key Laboratory of Powder Metallurgy, School of Materials Science and Engineering, Central South University, Changsha, 410083, People's Republic of China
[b] School of Engineering and Materials Science, Queen Mary University of London, Mile End Road London EI 4NS, United Kingdom

ARTICLE INFO

ABSTRACT

Boron-doped diamond (BDD) has proved to be an ideal anode material for the electrolysis of organic sewage. However, the existing two dimensional BDD electrodes with small active area and low mass transfer rates, limit their further improvement in degradation efficiency. In this paper, a novel three dimensional macroporous BDD (3D-BDD) foam electrode with a structure of evenly distributed pores and interconnected networks in which wastewater can flow freely was prepared using a simple and reproducible method. Compared to two dimensional BDD electrodes of the same geometry, the electro-active surface area of 3D-BDD electrode increased by ~20 times, and the electrochemical oxidation reaction rate constant of RB-19 increased by ~350 times. Under optimized conditions, the energy consumption reduced to a minimum of 0.03 kWh(gTOC)$^{-1}$, and the MCE reach a maximum of 325.86%.

1. Introduction

Since the last century, the treatment of wastewater produced by printing and dyeing, textile, pesticide, pharmaceutical, petrochemical and other industries has attracted much attention [1,2]. These industrial wastewater normally contain complex, chemically stable, and bio-refractory organic pollutants [1,3]. Due to their toxicity, carcinogenicity and mutagenicity, these organic pollutants are likely to cause some unimaginably disastrous consequences on the environment and human health even with low concentrations in water [4]. As a typical active anthraquinone dye, RB-19 was widely used in the printing and dyeing industry due to its strong chroma stability and good reproducibility. On the other hand, it has strong chemical stability (half-life cycle = ~46 years, pH = 7, T = 25 °C), non-biodegradability (50% < EC20 < 75%), toxicity and good water solubility [5], therefore RB-19 would remain in water for a very long time without an effective way of treatment. Unfortunately, traditional treatments like biochemical methods were proven to be ineffective [6].

Electrochemical Advanced Oxidation Processes (EAOPs), as a clean, effective and environmentally friendly electro-catalytic technology, is a research focus in the field of organic wastewater treatment in recent years [7,8]. Boron-doped diamond (BDD) is an ideal anode material for electrochemical oxidation processes due to its excellent mechanical properties, high oxidation potential, wide potential window, extremely low background current and good corrosion resistance [9]. Many studies have reported that RB-19 can be effectively removed by electro-catalytic oxidation with BDD electrodes [6,10,11].

The electro-catalytic activity of BDD is greatly affected by the characteristics of the electrode (including boron concentration, sp^3/sp^2 ratio, film thickness, surface termination, etc.), particularly by the surface roughness [12]. Because the rougher the surface, the larger effective electro-active surface area (EASA) will be, which not only increases the contact area between the sewage and the electrode, but also increases the active reaction sites for the generation of hydroxyl radicals (·OH) during electrolysis, thereby enhancing the oxidation efficiency of BDD electrode. Based on the above analysis, considerable research efforts have been devoted to the study of BDD electrodes with large EASA and their applications in the fields of electrochemical oxidation [9,13], supercapacitors [14], biosensors [15], solar cells [16] and so on. The preparation methods of BDD with high specific surface area are mainly divided into two types in principle: (i) etching the surface of BDD [13,17–20], and (ii) deposition on a porous template

---

[14,21–23]. Method of etching BDD usually first deposits a planar BDD film and then etches it to form a porous structure, including mask etching [17], high temperature activation [18,19], metal-assisted etching [13,20], etc. For example, Honda et al. produced BDD with honeycomb structures by oxygen plasma etching using porous alumina masks [17]. Kondo et al. obtained a structure with dense pores on BDD surface using a two-step method, graphitizing it at 1000 ℃ in argon atmosphere, then removing the graphite phase in air at 425 ℃ [19]. Li et al. obtained porous BDD films with nanopores of different shapes (including square and triangular) by Ni-nanoparticle-assisted plasma etching, and the EASA was 2.43 times larger than its geometric area [9]. However, there are some shortcomings in the method of BDD etching: one is the size of nanopores are difficult to control accurately, and it is a complex preparation process which is far from energy efficient, also the BDD could be easily contaminated by unnecessary masking metal impurities during the etching process [21]. Compared to etching process, depositing BDD films by chemical vapor deposition (CVD) on porous templates with large specific surface area is a better method. A number of works have been done on BDD to increase EASA by depositing diamond on various substrates such as carbon nanotubes [14], glass fiber [21,22] and porous silicon [23], etc. For example, Zanin et al. grown nanostructured BDD films on vertically aligned carbon nanotubes, as a result, the electrochemical active area and double-layer capacitance of the "teepee" structured BDD electrode are ~450 times greater than those of the planar BDD electrode [14]. Petrák et al. deposited BDD films on SiO_2 fibers by spin coating or doctor blade techniques on a planar BDD film, and then removed SiO_2 fibers by pickling to obtain a porous film [21]. However, so far as we know, the reported preparation methods of substrates with large specific area are complicated to operate. And since the size and depth of the pores are mostly in the nanometer order, namely they still belong to two-dimensional porous electrodes, not allowing organic wastewater to readily flow in and out through the channels of material. As a result, the electrochemical oxidation efficiency will be hindered by the limited diffusion. He et al. obtained a BDD foam electrode by depositing on a porous titanium substrate prepared by powder metallurgy, expanding the preparation of porous BDD from two dimensions to three dimensions, and endowed it three-dimensional pores and adjustable porosity [24]. However, the irregular shape, uneven distribution of the pores and the inhomogeneous small pore size (1–2 μm) make it difficult to obtain a continuous and uniform diamond film inside the substrate and cannot form through-type channels for organic wastewater to flow freely inside. So it still belongs to the plate electrode from the macroscopic, not helpful for the improvement of liquid mass transfer, resulting in the current efficiency is less than 30%, thus limits the further improvement of electrochemical oxidation efficiency [24].

Based on the above discussion, this paper aims to increase the EASA of BDD films and to improve the liquid phase mass transfer in the degradation process by a new method which is easy to operate, reproducible, and does not require complicated substrate preparation process. A novel three-dimensional BDD fully coated Ni foam electrode with adjustable pore size and interconnected channels in which wastewater can flow freely was prepared. In addition, the electrocatalytic performance and degradation mechanism of 3D-BDD electrode were studied by the degradation of refractory dye RB-19. This work has expanded the possibility of 3D design of high-quality three dimensional BDD electrodes and its application in actual wastewater treatment.
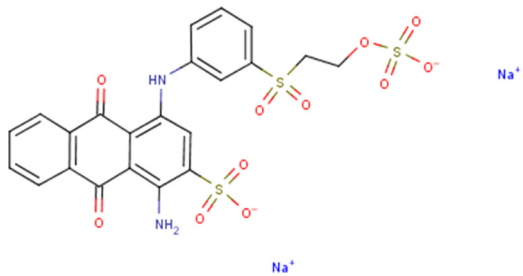
2. Experimental

2.1. preparation of BDD

Planar BDD (referred to be 2D-BDD) films were deposited on commercial titanium sheets of 20 mm × 30 mm × 1.5 mm using hot filament CVD technique in the mixed gas atmosphere for 24 h. The mixture of gas was in the ratio of B_2H_6(diluted by 95% of hydrogen) : CH_4 : H_2 = 0.2 sccm : 2 sccm : 98 sccm. B_2H_6 was used as the source of boron and the ratio of [B]/[C] was 10,000 ppm. The deposition system's temperature was kept at ˜850 ℃ and the pressure was maintained at 3 kPa.

A batch of high-quality three dimensional BDD foam (referred to be 3D-BDD) was made by two steps. Nickel foam (NF, porosity of 50 ppi) with the same geometry size of 2D-BDD was used as substrate since Ni has a good toughness as metal frame material and the mechanical stability of BDD can be assured. To match the thermal expansion coefficient of BDD, NF was coated with Ti interlayer through physical vapor deposition (PVD) technique. The magnetron sputtering (MS) conditions were set as follows: the power was 80 W, the pressure was kept at 0.5 Pa, and sputter time for the front side and the reverse side were 30 min, separately. Ti transition layer was sputtered in Ar atmosphere, the purity of the titanium target and argon gas was 99.99 wt% and 99.99 vol%, respectively. For better nucleation, both the substrates (flat Ti, NF) were put into the nanocrystalline diamond suspension for ultrasonic vibration of 30 min. The pretreatments for the substrates before deposition have been demonstrated in our previous work [25]. Then 3D-BDD films were deposited under the same conditions with 2D-BDD. Due to the differences of hot wire radiation distance along the thickness direction of 3D substrates, BDD film either cannot fully cover the hole areas or with a worse quality. Therefore, it is necessary to deposit BDD film on the front side for 12 h and then on the reverse side for 24 h.

2.2. Electrocatalysis of RB-19

Anthraquinone dye Reactive blue 19 (purity > 99%) was purchased from Shanghai 8th Dyestuff Chemical factory, its chemical structure

Table 1
Chemical structural and physical information of RB-19.

Commercial Name	Reactive blue 19
Chemical Structure	
Molecular Formula	$C_{22}H_{16}N_2Na_2O_{11}S_3$
Molar Mass	626.54 g/mol
CAS Number	2580-78-1

and physical information was listed in Table 1. Na$_2$SO$_4$ used as the supporting electrolyte was purchased from Shanghai Sinopharm Chemical Reagent Co., Ltd. All simulated dye wastewater was prepared with deionized water (resistivity of 18.25 MΩcm^{-1}) from a water purification system (UPT-I-10 T, Accexp company, China). Electrolysis of RB-19 was performed in a 0.5 L container with BDD as anode and a stainless steel of 20 mm × 30 mm as cathode. The distance of two electrodes set in parallel was kept in 1 cm. To ensure solution's appropriate mass transfer flow forward/to electrodes, a magnetic stirrer with rotating rate of 150 rpm was used during electrolysis process. The concentration of Na$_2$SO$_4$ was 0.1 M and the applied current was 0.3 A. To study the influence of dye initial concentration on 3D-BDD's electrolysis efficiency, the concentration of RB-19 was adjusted as 100 mg/L, 200 mg/L, 400 mg/L, respectively. Degradation experiments were performed in room temperature and the pH of solution was unadjusted.

2.3. Characterization

In this paper, the surface morphologies of 2D-BDD and 3D-BDD films were characterized using field emission scanning electron microscope (Nova NanoSEM 230, FEI, Netherlands). Raman spectra (wavelength of 488 nm, LabRAM HR800) were obtained to study the quality and doping level of diamond and X-ray diffraction (XRD, SIMENSD500, CuK_{α}) was used to characterize the grain orientation and phase composition. Cyclic voltammograms (CV) and electrochemical impedance spectra (EIS) were obtained by using electrochemical workstation (CHI660E, Shanghai CH Instrument Company, China) with a standard three-electrode system (2D-BDD or 3D-BDD served as a working electrode, a reference electrode Ag/AgCl and a platinum plate served as counter electrode) in solution of 0.1 M KCl and 0.01 mM K$_3$Fe(CN)$_6$. By analyzing CV curves under different sweep rates, the EASA of BDD films were calculated according to Randles-Sevcik Eq. (1) [9]:

$$I_{\mathrm{p}} = 2.69 \times 10^5 \cdot n^{3/2} A \cdot D^{1/2} \cdot C \cdot v^{1/2} \qquad (1)$$

Where I_{p} (A) is the peak current, n is the electron transfer number, D (cm^{2}s^{-1}) is the diffusion coefficient, C (molcm^{-3}) is the bulk concentration, v (Vs^{-1}) is the scan rate, and A (cm^2) is the EASA.

The removal of RB-19 and mineralization efficiency can be determined using a UV–vis spectrophotometer (UV-2600, Shimadzu, Japan) with a scanning range of 200–900 nm and a TOC analyzer (TOC-L, Shimadzu, Japan) by measuring the total organic carbon (TOC) of dye solution, respectively [8,26].

Mineralization current efficiency (MCE) and energy consumption (EC) of per unit weight can be calculated as follows [27,28]:

$$\mathrm{MCE}(100\%=) \frac{nFV_s \Delta[TOC]\exp}{4.32 \times 10^7 mIt} \times 100 \qquad (2)$$

Where n is the number of electrons for the mineralization of 1 mol RB-19 (n = 112), F is the Faraday constant (96,487 Cmol^{-1}), V$_s$ (L) is the solution volume, $\Delta[TOC]_{exp}$ (mgL^{-1}) is the experimental TOC decrement, m is the number of carbon atoms of RB-19 (m = 22), I (A) is the applied current and t is the treatment time (h) [29].

$$EC((kWh(gTOC))^{-1}) \frac{EIt}{V\Delta(TOC)_{exp}} \qquad (3)$$

Where E (V) is the average voltage of reaction vessel during the electrolysis process.

3. Results

3.1. Morphology of BDD electrodes

The morphologies of 2D-BDD, the inside holes and surface of 3D-BDD films were observed through SEM images in Fig. 1. Holes of 3D-BDD with a porosity of 50 ppi were evenly distributed and in regular shape. Diamond grown on surface and inside frame was continuous and uniform, fully coated by the three-dimensional foam skeletons without cracks or holes. The pore diameter was around 1 mm and the width of skeletons was around 200 μm (Fig. 1a). Due to the effect of hot filament radiation distance and a gradation of radicals and gas composition caused by the thickness of three-dimensional substrate, the average grain size of diamond grown on surface (4–5 μm) was slightly larger than on inside holes (2–3 μm). Fig. 1h-i shows the surface morphology of 2D-BDD grown under the same conditions. The diamond film grown continuously and densely, without holes or cracks, and the average grain size was 2–3 μm.

The carbon phase composition and boron-doping level of 3D-BDD's surface and inside skeletons were analyzed through Raman scattering spectra and compared to that of 2D-BDD. Three obvious bands can be seen at 475-490 cm^{-1}, 1204 cm^{-1} and 1315 cm^{-1} in Fig. 2. The broad peaks at 475-490 cm^{-1} and 1204 cm^{-1} can be attributed to the phonon scattering of lattice structural modifications caused by doped boron [30]. The boron atoms concentration of 3D-BDD and 2D-BDD were both estimated at ~10^{21} atoms cm^{-3} by using Lorenz fitting for Raman peaks at 475 cm^{-1} according to equation (S1), which was above the concentration of insulator to metal transition (~3 × 10^{20} atoms cm^{-3}), exhibiting the property of metal-like conductor [31].

Significant first-order diamond characteristic peaks at 1315 cm^{-1} can be seen in the Raman spectra of 3D-BDD and 2D-BDD films, showing that both films was dominated by sp^3 diamond and the quality of diamond grown on inside skeletons of 3D-BDD was not affected by the hot wire radiation gradient, which was consistent with what was observed from SEM. In addition, a asymmetry at lower frequencies of diamond peak was caused by boron doping at 1204 cm^{-1} which leads to Raman scattering relaxation of k = 0 selection rule and Fano effect [32]. It can be seen that the weak sp^2 carbon (graphite structure) characteristic band appears at ~1580 cm^{-1} in both BDD films, indicating the amount of non-diamond phase was very small.

In order to further understand the crystal orientation and phase composition, XRD spectra of 3D-BDD and 2D-BDD were compared in Fig. 3. Obvious diamond peaks assigned to (111) and (220) diffraction planes were appears at 2θ = 44.3° and 75.3°, respectively. It matches the observation from SEM and Raman spectra and further confirms the high quality of both BDD films. In addition, the peaks appears at 2θ = 63.1° and 76.1° in both XRD patterns was assigned to the (110) and (112) reflections of Ti phase, which was the transition layer of 3D-BDD and the substrate of 2D-BDD. Also, diffraction peaks at 2θ = 36.1° and 72.8° in both patterns were assigned to (111) and (311) reflections of TiC phase, which was formed by carbide of transition layer Ti. Compared to 2D-BDD, since the substrate of 3D-BDD was Ni, the XRD pattern has a Ni phase at 2θ = 51.8° and 76.4°, corresponding to the diffraction surface of (200), (220), respectively. Sputtered titanium is easily oxidized at room temperature, thus the transition layer Ti was oxidized to cause (211) and (321) diffraction planes peaks of TiO$_2$ at 2θ = 30.8° and 47.8°. Compared with the thin transition layer Ti of 3D-BDD, the XRD pattern of 2D-BDD shows more diffraction planes of Ti and TiC, such as peaks at 2θ = 35.2°, 40.3°, 53.1° and 70.8° which could be ascribed to (100), (101), (102), (103) reflections of Ti and peaks at 2θ = 41.9°, 60.8° were attributed to (200), (220) diffraction surfaces of TiC.

3.2. Electrochemical characterization

EASA is an important parameter for the electrochemical properties of an electrode. Fig. 4a, b shows the cyclic voltammograms of 3D-BDD and 2D-BDD electrodes at scan rates between 20-100 mVs^{-1} in 1 mM K$_3$Fe(CN)$_6$/K$_4$Fe(CN)$_6$, respectively. A good linear relationship was found taking the square root of scan rates as the abscissa and the peak current as the ordinate (Fig. 4a, b). The fitted linear equation of the 3D-BDD's peak current and the square root of scan rate can be written as I$_{PA}$ = 0.03956 $v^{1/2}$ + 6.36E-5(R^2 = 0.999), I$_{PC}$ = -0.03274 $v^{1/2}$ – 1.26E-3(R^2 = 0.999). As for 2D-BDD, the linear relation can be written
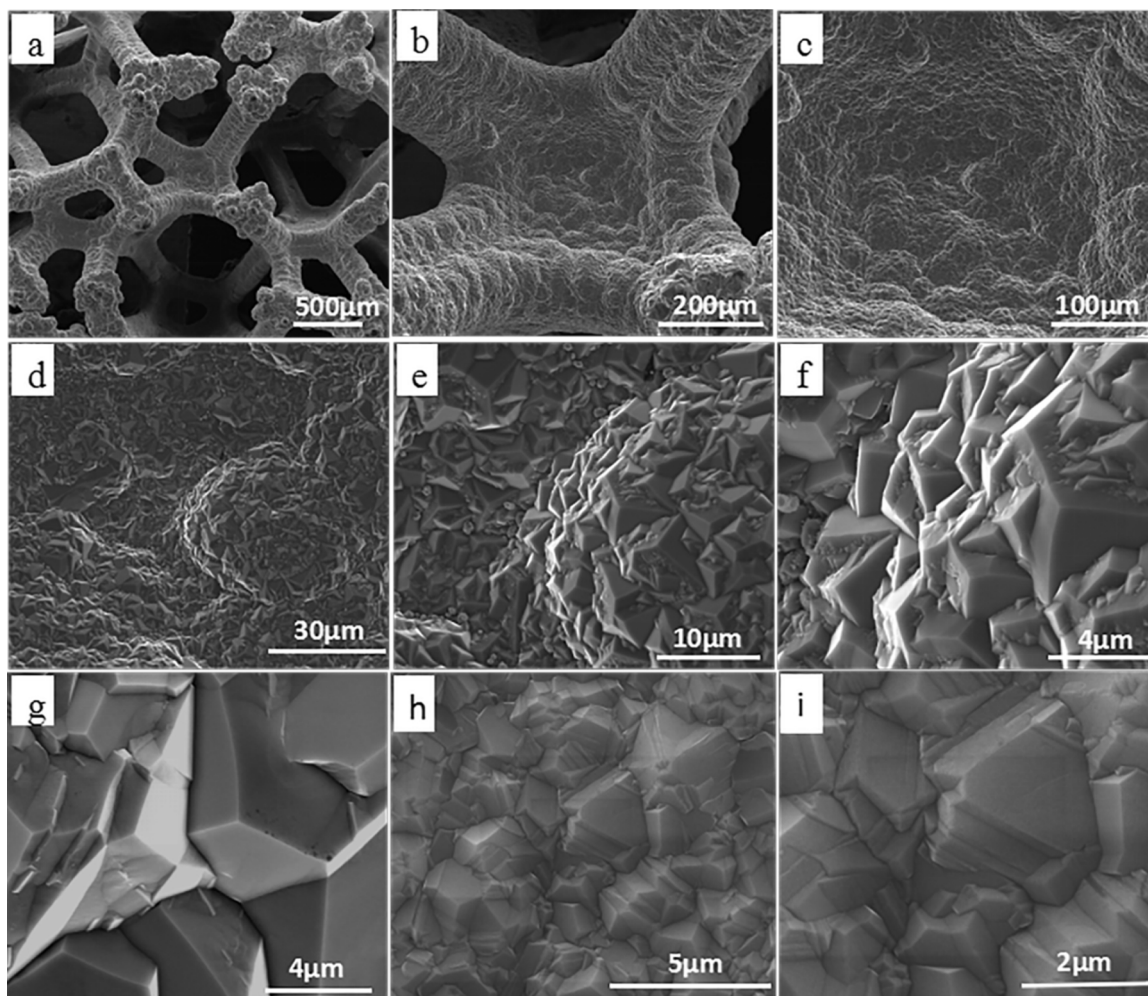
Fig. 1. SEM images of 2D-BDD and 3D-BDD electrodes. The SEM images of internal pores at different magnifications (a–f) and the surface (g) of 3D-BDD, (h–i) the SEM of 2D-BDD electrode at different magnifications.
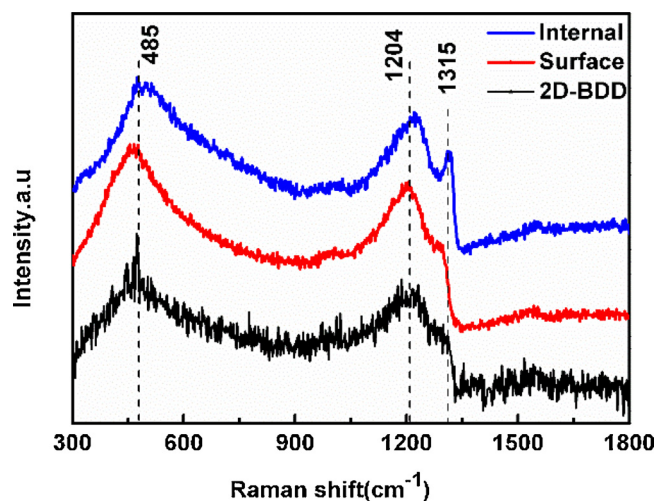

Fig. 2. Raman spectra of 2D-BDD and the internal skeleton, surface of 3D-BDD electrode.

Fig. 3. XRD diagram of 3D-BDD and 2D-BDD.

as $I_{PA} = 1.704E\text{-}4\ \nu^{1/2} + 7.078E\text{-}7(R^2 = 0.999)$, $I_{PC} = -1.716\ E\text{-}4\nu^{1/2} - 7.956E\text{-}7(R^2 = 0.999)$. This indicates that the diffusion process was the determining step of electrochemical reaction on the surface of the two BDD electrodes. According to the Randles-Sevcik Eq. (1), the EASA of 2D-BDD and 3D-BDD electrodes were calculated to be 6.21 cm^2

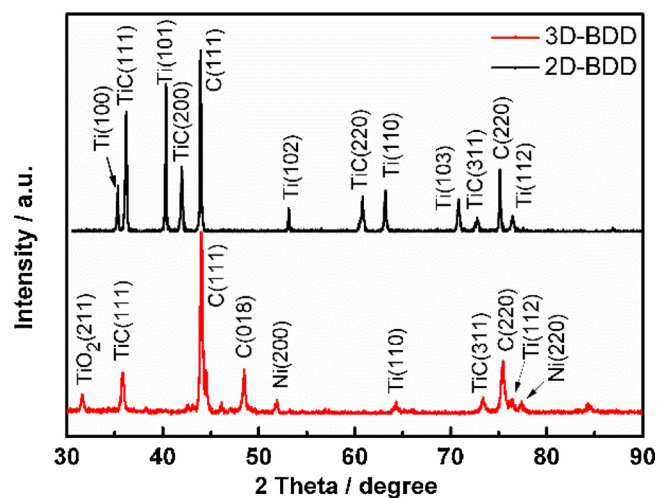(1.04 cm^2/cm^2) and 125.64 cm^2 (20.96 cm^2/cm^2), respectively. The EASA of 3D-BDD significantly increased by about 20 times compared to 2D-BDD electrode, which was consistent with the SEM observation that the 3D-BDD electrode surface and the internal skeleton were completely covered by high-quality BDD films. To compare the electrocatalytic performance of the two BDD electrodes, CV curves at the same scan rate
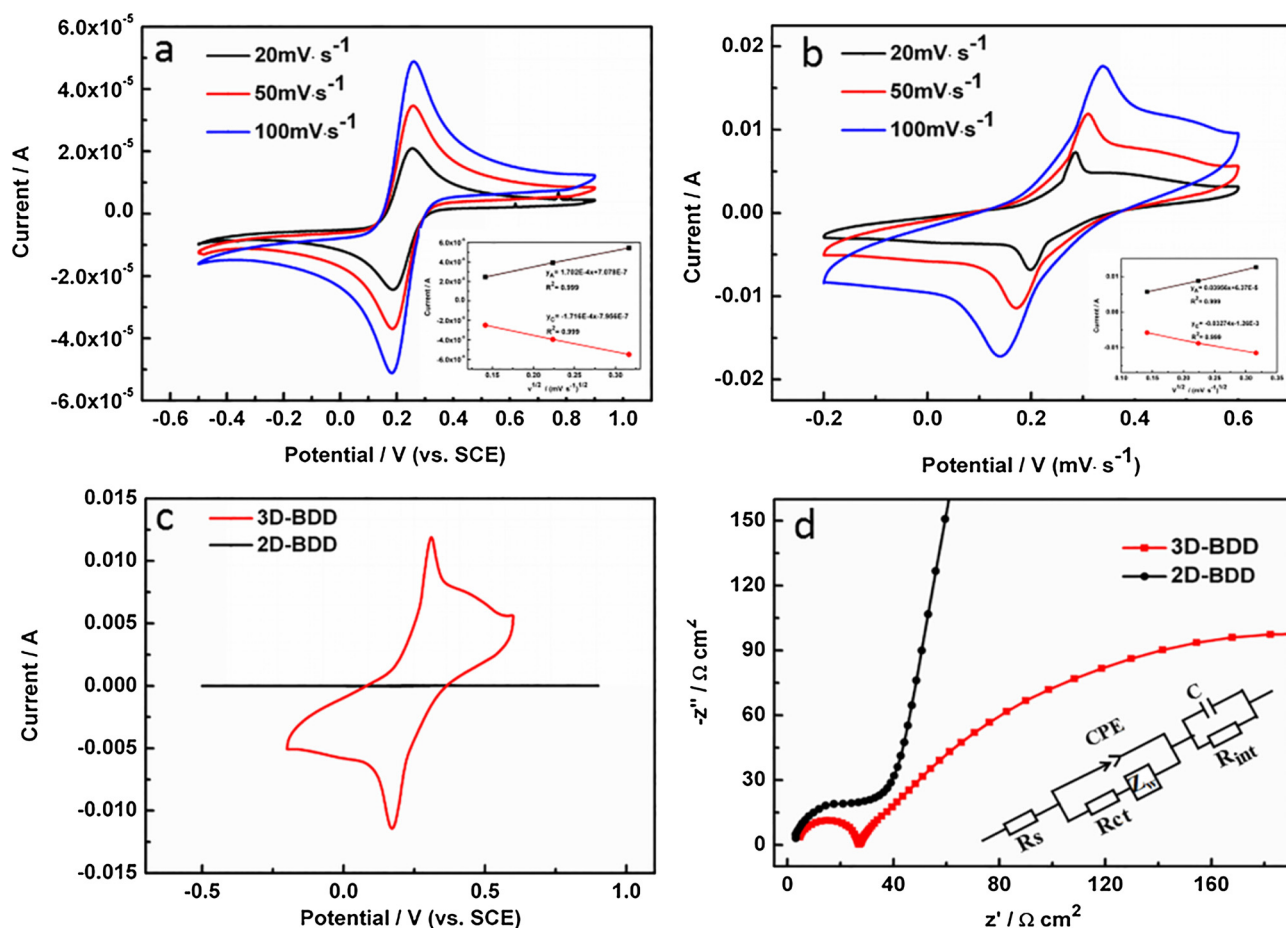
Fig. 4. Comparisons of the electrochemical effective area and electron transfer impedance of 3D-BDD and 2D-BDD electrode. The CV curves of 2D-BDD electrode (a) and 3D-BDD electrode (b) at different scan rates (20-50 mVs^{-1}), respectively, and a linear fit of the peak current to the square root of the scan rate. (c) Comparison of CV curves of 2D-BDD and 3D-BDD electrodes at a scan rate of 50 mVs^{-1}. (d) is the Nyquist curve for the 2D-BDD and 3D-BDD electrodes, and their equivalent circuit. The electrochemical tests were carried out in solution of 1 M KCl + 1 mM $K_3Fe(CN)_6$/$K_4Fe(CN)_6$.

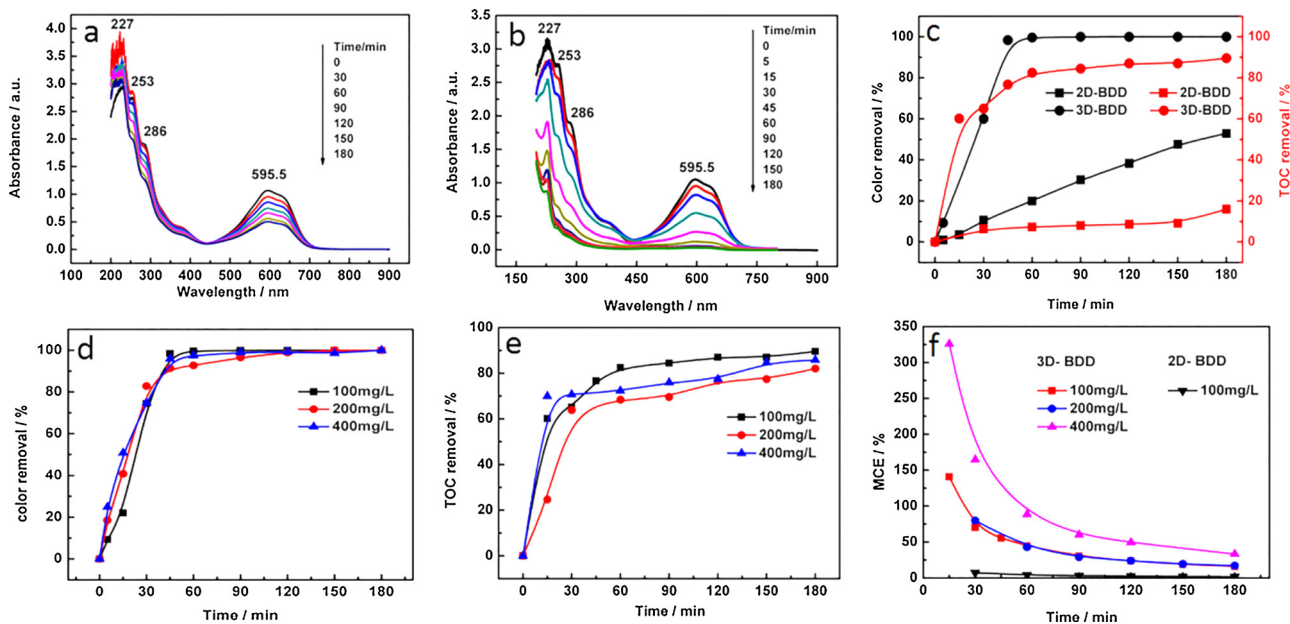**Fig. 5.** The UV–vis diagrams of 100 mg/L RB-19 using 2D-BDD (a) and 3D-BDD (b) electrodes. (c) Color removal and TOC removal of RB-19 (100 mg/L) as a function of degradation time with the two electrodes. Effect of RB-19 initial concentration (100, 200, 400 mg/L) on the degradation efficiency of 3D-BDD electrode : Color removal (d) and TOC removal (e). (f) The MCE of 2D-BDD and 3D-BDD at different degradation time.

of 50 mVs^{-1} were shown in Fig. 4c, and the oxidation/reduction peak current of 3D-BDD and 2D-BDD were 8.81E-3 A/-8.80E-3 A, 3.89E-5 A/-3.94E-5 A, respectively. The peak current value of 3D-BDD was 200 times of that of 2D-BDD exhibiting a significantly better electrochemical activity, which is attributed to the larger EASA of 3D-BDD electrode due to its three-dimensional porous structure.

To further analyze the electron transfer capacity in the solid-liquid interface of the two electrodes, EIS experiments were conducted to measure the electron transfer resistances (R_{ct}). Nyquist curves and their equivalent circuit were given in Fig. 4d. The equivalent circuit consists of a series resistor (R_s) and two parallel circuits. R_s and the first parallel circuit constitute a Randles circuit. The first parallel circuit includes an electron transfer resistance (R_{ct}), a constant phase element (CPE) and a Warburg resistance (Z_w). Rs was the resistance of electrode material. Since the surface of porous structure BDD electrode is not smooth, a CPE was used instead of the pure capacitor. The second parallel circuit includes an electric double-layer capacitor (C) of the solution and the internal solution medium resistance (R_{int}) of the system. The electrochemical parameters obtained by fitting the EIS experimental values to the equivalent circuit were listed in Table S1. According to the fitting results, the Rct of 2D-BDD and 3D-BDD electrodes were 38.89 Ωcm^2 and 22.26 Ωcm^2, respectively. Compared to 2D-BDD electrode, 3D-BDD electrode has a much lower charge transfer resistance. The greatly enhanced electrochemical performance of 3D-BDD electrode was beneficial to its electro-catalytic activity when degrading organic wastewater.

3.3. Electrochemical catalytic oxidation of RB-19

The electrochemical oxidation properties of the two electrodes were evaluated by taking RB-19 as the target organic contaminant. Fig. 5a,b showed the UV–vis spectra of RB-19 wastewater samples (initial concentration of 100 mg/L) treated by 2D-BDD and 3D-BDD electrodes. Four obvious peaks can be seen in both spectra. The characteristic peak of RB-19 appears at λ = 595.5 nm was caused by the transition of n→π* in the visible region, which can quantitatively reflect the removal of RB-19. The other three peaks in the near-ultraviolet region (λ = 227, 253, 286 nm) can be attributed to the π→π* transition of the aromatic structure. It can be seen that all the peaks in the UV–vis spectrum of the 3D-BDD electrode decreased much sharper than 2D-BDD. Comparing the color removal rate and TOC removal rate of the two electrodes (Fig. 5c), the degradation and mineralization rates of RB-19 by 3D-BDD electrode were significantly higher than those of 2D-BDD electrode. After a treatment of 120 min at a small current of 0.3 A, the color removal and TOC removal of RB-19 by 2D-BDD and 3D-BDD electrodes reached 30.82%, 100%, 8.03% and 87.02%, respectively. According to the formula ($Ln (C_0/C_t) = k \times t$, where C_0, C_t was the concentration of RB-19 at initial stage and after degradation time t, and k was the rate constant for the first-order reaction kinetics), the kinetic rate constants for RB-19 degradation with 2D-BDD and 3D-BDD electrodes (Fig. S1) were calculated as k = 0.0042 min^{-1} (R^2 = 0.99) and k = 1.487 min^{-1} (R^2 = 0.99), respectively. Compared to 2D-BDD, the reaction rate constant of 1.487 min^{-1} of 3D-BDD electrode significantly increased by ~350 times with a small applied current density of 50 mA/cm^2. Encouragingly, as far as we know, it is the highest reaction rate of electrochemical oxidation of BDD electrodes ever reported ones under these conditions [9,33–35].

Fig. 5d, e shows the time variation of color removal and TOC removal of RB-19 treated by 3D-BDD electrode at three initial concentrations. The results show that the increase of the dye concentration has little effect on the degradation rate of RB-19, and all of them can reach more than 90% of color removal within 1 h. The removal of total organic carbon is a process in which organic matter is completely oxidized into carbon dioxide and inorganic matter, reflecting the mineralization degree of organic pollutants, thereby the complete TOC removal is more difficult to obtain than the color removal. The

electrochemical degradation experiment of RB-19 at high concentration (400 mg/L) still maintains a similar high mineralization efficiency (more than 60% TOC removal rate in 30 min) with low concentration (100 mg/L). Many papers [36] have studied the influence of initial concentration on the process efficiency and the uniform conclusion shows that higher initial concentration needs longer electrolysis time to achieve the same color removal or mineralization. This is because when the dye concentration increases, ·OH can't completely reflect organic matter near the surface of BDD in a short period of time, the saturated efficiency of BDD leads to lower mineralization rate. While in this article, when RB-19 dye concentration increased from 100 mg/L to 400 mg/L, the color removal and TOC removal after the same degradation time were similar, showed that due to the enhancement of electro-active surface area and mass transfer rate, the degradation efficiency of 3D-BDD electrode has been greatly promoted. Based on the conclusion obtained from our previous work [25] that BDD electrodes with the best electro-catalytic property toward simulated dye wastewater will exhibit the lowest sensitivity to degradation parameters in terms of simulated dye wastewater degradation, we can get a further confirmation of the excellent electro-catalytic performance of 3D-BDD. Fig. 5f compares the time variation of MCE with 2D-BDD and 3D-BDD electrode. The MCE of 3D-BDD electrode has a significant improvement compared to 2D-BDD electrode. After a treatment of 60 min and the mineralization rate of organic wastewater reached as high as 60–82.8%, the MCE of 3D-BDD still remains above 50%. MCE of 3D-BDD increased with the increase of initial concentration, especially during the degradation of 400 mg/L RB-19, the MCE of the electrode reached a maximum of 325.86% (t = 15 min). All degradation processes show a decrease in MCE with treatment time, which can be explained by the electrocatalysis with BDD was a diffusion process control reaction. At the initial stage of degradation, the dye concentration at the solid-liquid interface near by the electrode was high, and the organic substance can fully react with the short-lived strong oxidizing substances (such as ·OH) generated on the electrode surface, or be directly oxidized by the electrode, and thus the current efficiency was high. With the degradation time going by, the diffusion process limits the rapid supplement near the electrode, the concentration of organic matter decreases and oxygen evolution side reaction [37] with the excess ·OH increases, thus leading the utilization of short-lived oxidizing substances and the efficiency of direct oxidation on electrode surface decreases, resulting in a decrease in MCE in the electro-catalytic process.

Table 2 compared the energy consumption of 2D-BDD and 3D-BDD electrodes for electrochemical treatment of RB-19. After electrochemical treatment by 3D-BDD at 0.3 A for 1 h, the mineralization for RB-19 of 100, 200, and 400 mg/L reached 82.5%, 68.4%, 70.7% with EC of 0.19, 0.09, 0.05 kWh(gTOC)$^{-1}$, respectively. By comparison, the 2D-BDD electrode electrochemically degraded RB-19 of 100 mg/L for 1 h, the TOC removal of the dye was only 16.04% with a high EC of 1.871 kWh(gTOC)$^{-1}$. The degradation efficiency of 3D-BDD electrode was almost unaffected but the EC decreased with the increase of initial concentration, indicating that 3D-BDD electrode has a more obvious advance in treating organic wastewater at high concentrations.

To further illustrate the superior electrochemical performance of the 3D-BDD electrode, Table 3 summarizes the electrochemical degradation efficiency and corresponding EC of the 3D-BDD electrode with other BDD electrodes degrading RB-19 and BDD with large EASA that have been reported. It can be seen that the 3D-BDD with a higher degradation efficiency but a lower EC show an excellent electro-catalytic performance among all BDD electrodes. Petrucci et al. [6] reported a TOC removal of 7% after a 370 min treatment of synthetic organic wastewater containing 50 mg/L RB-19 under the optimized current density, and consumed more than 3000 C of electricity. Whereas in this paper, a much higher TOC removal (82.5%) of 100 mg/L RB-19 was obtained in 60 min, the processing time was shorten by 2/3, and the electricity consumption (1080 C) was only 1/3 of that. Degaki et al. [35] studied the degradation of 500 mg/L RB-19 containing 0.1 molL^{-1} Na$_2$SO$_4$ and

Table 2

Energy consumption and electricity with different initial dye concentrations.

Anode	Concentration (mg/L)	Color removal (%)	TOC removal (%)	EC (kWh(gTOC)$^{-1}$)	Q (AhL^{-1})
3D-BDD	100	60.0	65.0	0.12	0.3
		99.6	82.5	0.19	0.6
		100	89.6	0.45	1.8
	200	40.7	24.7	0.13	0.15
		82.8	68.4	0.09	0.3
		99.0	82.0	0.39	1.8
	400	50.8	70.0	0.03	0.15
		74.7	70.7	0.05	0.3
		100	85.81	0.25	1.8
2D-BDD	100	20	16.0	1.87	1.8

34 mmolL^{-1} NaCl with Nb/BDD, and found that a mineralization of 65% was reached with a electricity consumption of 8 Ah L^{-1}, without the existence of Cl-, a color removal of 98% needs to consume 5.5 Ah L^{-1}. Whereas a mineralization of 70.7% and a color removal of 100% of 400 mg/L RB-19 only consume electricity of 0.6 Ah L^{-1} and 1.8 Ah L^{-1} in this paper.

4. Discussion

Macroporous 3D-BDD foam electrodes with three-dimensional interconnected (mm) network structure were constructed in this paper. It can be seen from SEM and Raman characterization that the quality of BDD was not affected by the three-dimensional structure substrate. The EASA of 3D-BDD was increased by ~20 times comparing to the planar BDD of the same volume, which will greatly improve the space utilization when applied to practical wastewater treatment device. 3D-BDD electrode exhibits excellent electro-catalytic performance of high efficiency, high MCE and low EC in the degradation process of RB-19. The highest reaction rate constant of 1.487 min^{-1} has obtained with 3D-BDD electrode under the same degradation conditions as currently known, which benefits from (i) the large EASA caused by its three-dimensional porous structure and (ii) the liquid-flow channels formed by the interconnected macroporous network. On one hand, the increase of EASA per unit volume not only increases the contact area between the organic substance and the electrode surface, increasing the efficiency of direct oxidation, but also increases the active sites for the generation of the oxidizing substance, increasing the efficiency of indirect oxidation. On the other hand, from the point of view of dynamics, it is important to highlight that BDD electrochemical degradation of organic wastewater is a process controlled by the liquid-phase mass transfer steps (Fig. 4a-b). Liquid phase mass transfer limitation was a key factor that restricts the enhancement of MCE and degradation rate of BDD electrode. This is also an unresolved defect of other porous BDD electrodes that have been reported [24]: although the increased EASA of electrodes enhanced the generation rate of strong oxidizing substances (such as ·OH), but due to the restriction of small pore size (μm, nm) and

the depth of the pores, the mass transfer near the electrode surface was limited, leading to a low utilization of the transient ·OH and the advance of the large effective active area was not fully exerted. As for the 3D-BDD in our work, due to the three-dimensional interconnected network with much larger pore size (~1 mm), the penetrating channels for liquid circulation is big enough to overcome the resistance of very thin film of liquid near the solid film, in addition, the degradation process maintained a certain liquid-solid convection with a magnetic stirrer, making the flow state near the surface of electrode change from stagnation to turbulention and wastewater can flow freely through the 3D-BDD electrode. Compared to the laminar flow near the surface of the 2D-BDD electrode, the ascension of liquid phase mass transfer rate of 3D-BDD will improve the utilization rate of oxidants ·OH and large EASA, so as to improve the current efficiency and the degradation efficiency of the electrode. The conclusion that network structure can increase the mass transfer rate has been described in many reports [38]. The increase in the utilization of hydroxyl radicals caused by the increase in the mass transfer rate was confirmed by its extremely high MCE. Compared with the 2D-BDD electrode, the MCE of the 3D-BDD electrode increased by a hundred times at most, which was not only the effect of large EASA of the electrode (increased by ~20 times). Therefore, the existences of the penetrating channels are greatly helpful to the improvement of BDD efficiency, which is also one of the biggest novelties in this paper.

Compared to etching and other reported methods, the preparation of 3D-BDD using nickel foam as the substrate and sputtered Ti as the transition layer was not only much simpler to handle and lower in cost, but also can easily adjust the microstructure and porosity of BDD foam by controlling the geometry, pore size and porosity of the substrate. In addition, compared with other methods like electroplating, magnetron sputtering technology has its advances such as strong binding force, uniform density and high surface activity. The transition layer Ti film obtained by MS technology has a strong binding force with matrix Ni. Also, the high surface activity is beneficial for the nucleation and growth of diamond in the CVD process [39,40]. The high-quality 3D-BDD's novel three-dimensional macroporous interconnected network

Table 3

Comparison of efficiencies and EC of electrochemical degradation between 3D-BDD electrodes and other reported electrodes.

BDD	Dye	Degradation conditions			Removal/%		EC or charge	Ref.
		C_0	pH	Ce	CR	M		
3D	RB-19	400	–	0.1 M Na$_2$SO$_4$	74.7	70.7	0.05 [a]	In this paper
2D	RB-19	100	2.5	0.1 M K$_2$SO$_4$	97	35	0.17 [a]	[43]
2D	RB-19	500	6	0.01M Na$_2$So$_4$	98	–	5.5 [b]	[11]
2D	4-hydroxyphenylacetic acid	1.03mM	3	0.05 M Na$_2$SO$_4$	–	69.1	0.33 [a]	[44]
BDDNW	phenol	1mM	–	0.5 M Na$_2$SO$_4$	–	85	2.5 [b]	[13]
porous	phenol	114	2	0.5 M Na$_2$SO$_4$	85	–	2.78 [b]	[24]
porous	xylenol orange	103	2	0.5 M Na$_2$SO$_4$	85	–	2.52 [b]	[24]
3D-Ti/BDD	aspirin	100	–	0.5 M Na$_2$SO$_4$	100	–	2.7 [b]	[45]

Where C_0: the initial concentration of dye (mg/L); Ce: the concentration of electrolyte (M); CR: color removal; M: mineralization; a: EC (kWh(gTOC)$^{-1}$) and b: charge (C).

structure endows it exclusive advantages like large EASA, small electron transfer resistance, excellent electro-catalytic performance, high space utilization and fluid-flow channels, that BDD of two-dimensional structure does not have. From the electrolysis results, we can see that 3D-BDD electrode displayed excellent performance in organic wastewater treatment. If several 3D-BDD electrodes are assembled together, a real wastewater treatment device with advances including lightweight, small volume, high efficiency and low energy consumption can be constructed, which will have a very broad application prospect in the refractory organic wastewater. In addition to being applied in wastewater treatment, 3D-BDD is also promising for biosensor because its large EASA and thus enhanced electrochemical sensitivity [41]. Moreover, 3D-BDD electrodes are also great potential in the field of super capacitor [42] since the EASA is also crucial factor for that. In summary, the simple, reproducible and low-cost preparation of 3D-BDD electrode will accelerate the pace of industrialization of BDD in various applications such as wastewater treatment, biosensor, and super capacitor.

5. Conclusions

In this paper, high-quality 3D-BDD electrodes with uniformly distributed pores were obtained by CVD deposition on Ni foams. The diameters of pores were 1 mm and the skeleton width was 200 μm, forming interconnected channels through which the liquid phase can flow freely. The EASA of 3D-BDD electrode reaches 20.96 cm^2/cm^2, which was 20 times of that of 2D-BDD electrode. The peak current of the 3D-BDD electrode at the same sweep rate was much higher (200 times) and the electron transfer resistance was much lower than that of 2D-BDD electrode, showing a better electro-catalytic activity. Large EASA, small electron transfer resistance and fluid-flow channels, making 3D-BDD electrode exhibit excellent electrocatalytic oxidation performance in RB-19 treatment. The reaction rate constant k of the 3D-BDD electrode degrading RB-19 reached 1.487 min^{-1}, which was the highest value that have ever been reported under the same conditions. At a small current of 0.3 A, the color removal of 100% and the mineralization rate of 84.46% can be achieved in 90 min. The increase of dye concentration had little effect on the degradation efficiency of 3D-BDD electrode but enhanced the MCE and reduced EC. Especially when the initial concentration of RB-19 increased to 400 mg/L, the EC was as low as 0.03 $kWh(gTOC)^{-1}$ and the MCE reached a maximum of 325.86%. The high-quality 3D-BDD electrode not only opens the door to new possibilities in practical organic wastewater treatment of high-efficiency and low-EC, but also has broad application prospects in the fields of super capacitors and biosensors.

Appendix A. Supplementary data

Supplementary material related to this article can be found, in the online version, at doi:https://doi.org/10.1016/j.apcatb.2018.12.074.

References

[1] C. Salazar, N. Contreras, H.D. Mansilla, J. Yáñez, R. Salazar, J. Hazard. Mater. 319 (2016) 84–92.
[2] E.C. Paz, L.R. Aveiro, V.S. Pinheiro, F.M. Souza, V.B. Lima, F.L. Silva, P. Hammer, M.R.V. Lanza, M.C. Santos, Appl. Catal. B Environ. 232 (2018) 436–445.
[3] M. Schriks, M.B. Heringa, V.D.K. Mm, V.P. De, A.P. van Wezel, Water Res. 44 (2010) 461–476.
[4] A.C. Johnson, M.D. Jürgens, R.J. Williams, K. Kümmerer, A. Kortenkamp, J.P. Sumpter, J. Hydrol. 348 (2008) 167–175.
[5] E.J. Weber, V.C. Stickney, Water Res. 27 (1993) 63–67.
[6] E. Petrucci, D. Montanaro, Chem. Eng. J. 174 (2011) 612–618.
[7] I. Sirés, E. Brillas, M.A. Oturan, M.A. Rodrigo, M. Panizza, Environ. Sci. Pollut. R. 21 (2014) 8336–8367.
[8] C.A. Martínez-Huitle, E. Brillas, Appl. Catal. B Environ. 166-167 (2015) 603–643.
[9] X. Li, H. Li, M. Li, C. Li, D. Sun, Y. Lei, B. Yang, Carbon 129 (2018) 543–551.
[10] D. Montanaro, E. Petrucci, Chem. Eng. J. 153 (2009) 138–144.
[11] A.H. Degaki, G.F. Pereira, R.C. Rocha-Filho, N. Bocchi, S.R. Biaggio, Electrocatalysis 5 (2014) 8–15.
[12] P. Cañizares, C. Sáez, F. Martínez, M.A. Rodrigo, Electrochem. Solid St. 11 (2008) E15–E19.
[13] C.H. Lee, E.S. Lee, Y.K. Lim, K.H. Park, H.D. Park, D.S. Lim, RSC Adv. 7 (2017) 6229–6235.
[14] H. Zanin, P.W. May, D.J. Fermin, D. Plana, S.M. Vieira, W.I. Milne, E.J. Corat, ACS Appl. Mater. Interfaces 6 (2014) 990–995.
[15] Z. Deng, H. Long, Q. Wei, Z. Yu, B. Zhou, Y. Wang, L. Zhang, S. Li, L. Ma, Y. Xie, Actuator B-Chem. 242 (2016) 825–834.
[16] W.S. Yeap, D. Bevk, X. Liu, H. Krysova, A. Pasquarelli, D. Vanderzande, L. Lutsen, L. Kavan, M. Fahlman, W. Maes, RSC Adv. 4 (2014) 50678-50678.
[17] K. Honda, T.N. Rao, D.A. Tryk, A. Fujishima, M. Watanabe, K. Yasui, H. Masuda, J. Electrochem. Soc. 148 (2001) A668–A679.
[18] T. Ohashi, J. Zhang, Y. Takasu, W. Sugimoto, Electrochim. Acta 56 (2011) 5599–5604.
[19] T. Kondo, Y. Kodama, S. Ikezoe, K. Yajima, T. Aikawa, M. Yuasa, Carbon 77 (2014) 783–789.
[20] H.A. Mehedi, J.C. Arnault, D. Eon, C. Hébert, D. Carole, F. Omnes, E. Gheeraert, Carbon 59 (2013) 448–456.
[21] V. Petrák, Z.V. Živcová, H. Krýsová, O. Frank, A. Zukal, L. Klimša, J. Kopeček, A. Taylor, L. Kavan, V. Mortet, Carbon 114 (2017) 457–464.
[22] S. Ruffinatto, H.A. Girard, F. Becher, J.C. Arnault, D. Tromson, P. Bergonzo, Diam. Relat. Mater. 55 (2015) 123–130.
[23] V. Baranauskas, D.C. Chang, B.B. Li, A.C. Peterlevitz, V.J. Trava-Airoldi, E.J. Corat, R.K. Singh, D.G. Lee, J. Porous Mat. 7 (2000) 401–405.
[24] Y. He, W. Huang, R. Chen, W. Zhang, H. Lin, Sep. Purif. Technol. 149 (2015) 124–131.
[25] R. Mei, C. Zhu, Q. Wei, L. Ma, W. Li, B. Zhou, Z. Deng, Z. Tong, G. Ouyang, C. Jiang, J. Electrochem. Soc. 165 (2018) H324–H332.
[26] A. Bedollaguzman, R. Feriareyes, S. Gutierrezgranados, J.M. Peraltahernández, Environ. Sci. Pollut. R. 24 (2016) 1–9.
[27] A. Thiam, I. Sirés, J.A. Garrido, E. Brillas, Sep. Purif. Technol. 140 (2015) 43–52.
[28] S. Garcia-Segura, E. Brillas, Water Res. 45 (2011) 2975–2984.
[29] J.R. Steter, E. Brillas, I. Sirés, Electrochim. Acta 222 (2016) 1464–1474.
[30] P. Ashcheulov, J. Šebera, A. Kovalenko, V. Petrák, F. Fendrych, M. Nesládek, A. Taylor, Z.V. Živcová, O. Frank, L. Kavan, Eur. Phys. J. B 86 (2013) 443–451.
[31] R. Ramamurti, M. Becker, T. Schuelke, T. Grotjohn, D. Reinhard, G. Swain, J. Asmussen, Diam. Relat. Mater. 17 (2008) 481–485.
[32] D. Kumar, M. Chandran, M.S.R. Rao, Appl. Phys. Lett. 110 (2017) 013503-012853.
[33] Z. Frontistis, D. Mantzavinos, S. Meriç, J. Environ. Manage. 223 (2018) 878–887.
[34] N. Barhoumi, H. Olvera-Vargas, N. Oturan, D. Huguenot, A. Gadri, S. Ammar, E. Brillas, M.A. Oturan, Appl. Catal. B Environ. 209 (2017) 637–647.
[35] M. Ghazouani, H. Akrout, S. Jomaa, S. Jellali, L. Bousselmi, J. Electroanal. Chem. 783 (2016) 28–40.
[36] E.M. Siedlecka, A. Ofiarska, A.F. Borzyszkowska, A. Bialk-Bielinska, P. Stepnowski, A. Piecznska, Water Res. 144 (2018) 235–245.
[37] H. Song, L. Yan, J. Jiang, J. Ma, Z. Zhang, J. Zhang, P. Liu, T. Yang, Water Res. 128 (2017) 393–401.
[38] H. Xu, W.M. Huang, Y. Xing, H.B. Lin, H.H. Ji, M. Jiang, X.B. Liu, S.C. Gan, Chin. J. Chem. Eng. 16 (2008) 198–202.
[39] Q. Wei, T. Yang, K.C. Zhou, L. Ma, P. Zheng, J. Li, D. Zhang, Z. Li, Z.M. Yu, Surf. Coat. Technol. 232 (2013) 456–463.
[40] W. Ye, Q. Wei, L. Zhang, H. Li, J. Luo, L. Ma, Z. Deng, C.-T. Lin, K. Zhou, Mater. Des. 156 (2018) 32–41.
[41] W. Dai, H. Li, M. Li, C. Li, X. Wu, B. Yang, ACS Appl. Mater. Interfaces 7 (2015) 22858–22867.
[42] S. Yu, N. Yang, M. Vogel, S. Mandal, O.A. Williams, S. Jiang, H. Schoenherr, B. Yang, X. Jiang, Adv. Energy Mater. 8 (2018) 1702947.
[43] V.M. Vasconcelos, F.L. Migliorini, J.R. Steter, M.R. Baldan, N.G. Ferreira, J. Environ. Chem. Eng. 4 (2016) 3900–3909.
[44] N. Flores, I. Sirés, R.M. Rodríguez, F. Centellas, P.L. Cabot, J.A. Garrido, E. Brillas, J. Electroanal. Chem. Lausanne (2017) 58–65.
[45] Y. He, W. Huang, R. Chen, W. Zhang, H. Lin, J. Electroanal. Chem. 758 (2015) 170–177.